Stability of $Ar(H_2)_2$ to 358 GPa

HPSTAR 349-2017

Cheng Ji[a,b], Alexander F. Goncharov[c,d], Vivekanand Shukla[e], Naresh K. Jena[e], Dmitry Popov[b], Bing Li[a,f,g], Junyue Wang[a,c], Yue Meng[b], Vitali B. Prakapenka[h], Jesse S. Smith[b], Rajeev Ahuja[e], Wenge Yang[a,g], and Ho-kwang Mao[a,c,1]

[a]Center for High Pressure Science and Technology Advanced Research, Shanghai 201203, China; [b]High Pressure Collaborative Access Team, Geophysical Laboratory, Carnegie Institution of Washington, Argonne, IL 60439; [c]Geophysical Laboratory, Carnegie Institution of Washington, Washington, DC 20015; [d]Key Laboratory of Materials Physics, Institute of Solid State Physics, Chinese Academy of Sciences, Hefei 230031, China; [e]Condensed Matter Theory, Materials Theory Division, Department of Physics and Astronomy, Uppsala University, S-75120 Uppsala, Sweden; [f]Center for the Study of Matter at Extreme Conditions, Department of Mechanical and Materials Engineering, Florida International University, Miami, FL 33199; [g]High Pressure Synergetic Consortium, Geophysical Laboratory, Carnegie Institution of Washington, Argonne, IL 60439; and [h]Center for Advanced Radiation Sources, University of Chicago, Argonne, IL 60439

Contributed by Ho-kwang Mao, February 9, 2017 (sent for review January 3, 2017; reviewed by Renata M. Wentzcovitch and Choong-Shik Yoo)

"Chemical precompression" through introducing impurity atoms into hydrogen has been proposed as a method to facilitate metallization of hydrogen under external pressure. Here we selected $Ar(H_2)_2$, a hydrogen-rich compound with molecular hydrogen, to explore the effect of "doping" on the intermolecular interaction of H_2 molecules and metallization at ultrahigh pressure. $Ar(H_2)_2$ was studied experimentally by synchrotron X-ray diffraction to 265 GPa, by Raman and optical absorption spectroscopy to 358 GPa, and theoretically using the density-functional theory. Our measurements of the optical bandgap and the vibron frequency show that $Ar(H_2)_2$ retains 2-eV bandgap and H_2 molecular units up to 358 GPa. This is attributed to reduced intermolecular interactions between H_2 molecules in $Ar(H_2)_2$ compared with that in solid H_2. A splitting of the molecular vibron mode above 216 GPa suggests an orientational ordering transition, which is not accompanied by a change in lattice symmetry. The experimental and theoretical equations of state of $Ar(H_2)_2$ provide direct insight into the structure and bonding of this hydrogen-rich system, suggesting a negative chemical pressure on H_2 molecules brought about by doping of Ar.

ultrahigh pressure | hydrogen-rich compound | intermolecular interaction | metallization

Chemistry under extreme conditions continues to inspire generations of researchers as it charts excitingly new realms of structures, properties, and phenomena in molecular systems (1). As an extreme case of tuning properties of simple molecules using pressure, metallic hydrogen has been keenly pursued for decades due to the predicted intriguing properties, i.e., room-temperature superconductivity (2) and superfluidity (3), and its fundamental scientific implications (4–6). However, for solid hydrogen, neither the predicted metallization in the atomic form through molecular dissociation (7) nor that in the molecular form through bandgap closure (8) has been achieved experimentally up to ∼400 GPa (9, 10). This is almost the pressure limit of studying solid hydrogen using the current static high-pressure techniques.

It has been proposed theoretically that the attainment of metallic hydrogen can be facilitated through chemical precompression in the form of hydrogen-rich materials (11–13). As one of the hydrogen-rich van der Waals compounds found under high pressure (14–19), $Ar(H_2)_2$ has been considered as a viable candidate. An experimental study revealed a phase transition of $Ar(H_2)_2$ associated with a molecular dissociation and possible Drude-type metallic behavior above 175 GPa at 100 K (20). A follow-up high-pressure IR absorption study up to 220 GPa at 100 K showed a persistence of molecular H_2 questioning the proposed metallization (21). Further theoretical studies of $Ar(H_2)_2$ also showed conflicting results. New phases were predicted at pressures ranging from 55 to 250 GPa (22–24). Based on different crystal structures, some calculation predicted metallization at lower pressure (22), whereas others suggested delayed metallization compared with pure H_2 (23–25). Due to a lack of clear structural information at very high pressures, these theoretical calculations of electronic structure were hampered and have yet to be verified.

Here we report high-pressure synchrotron X-ray diffraction (XRD) and Raman spectroscopy experiments up to 358 GPa supplemented by density-functional theory (DFT)-based computations, elucidating the structure and bonding of $Ar(H_2)_2$ and clearly addressing previous inconsistencies. Our studies show stability of insulating $Ar(H_2)_2$ with the $MgZn_2$-type structure in the pressure range up to at least 265 GPa based on XRD and to 358 GPa based on continuity of optical spectroscopy observations. A splitting of the H_2 vibron recorded above 216 GPa points to a molecular orientational ordering transition. The structure and equation of state (EOS) of $Ar(H_2)_2$ were used to understand the effect of Ar doping on the molecular interaction of H_2, suggesting that Ar doping introduces a negative chemical pressure on H_2 molecules.

At pressure above 4.2 GPa, $Ar(H_2)_2$ was observed to crystallize from a mixture of Ar and H_2 in a diamond anvil cell (DAC), consistent with the previous reports (20, 26). A refinement of the single-crystal XRD (SXRD) data collected at 8.1 GPa was performed based on the proposed $MgZn_2$-type structure model, which has a hexagonal close-packed lattice with H_2 molecules occupying two crystallographic sites (20). The refinement gives excellent results, R1 = 3.77%. We observed a presence of weak diffraction rods in some samples with certain crystal orientation, which may indicate some disorder in atomic positions. *SI Appendix* includes details about SXRD refinement and diffraction rods.

Significance

Pressure-induced metallization of solid hydrogen is a problem of certain prominence in high-pressure physics. However, it is extremely challenging to be achieved experimentally. It was proposed that "chemical precompression" (introducing impurity atoms or molecules into hydrogen) may facilitate metallization under pressure. In this paper, we selected $Ar(H_2)_2$ as a model system and explored the intermolecular interactions of H_2 molecules and the metallization of hydrogen in the presence of a weakly bound impurity (Ar). Combining our experimental data and theoretical calculations, we found that Ar does not facilitate the molecular dissociation and bandgap closure of H_2, moreover it works in the opposite direction. Our work provides a solid basis for future searches of hydrogen-rich materials which facilitate metallization of hydrogen.

Author contributions: R.A. and H.-k.M. designed research; C.J., V.S., N.K.J., B.L., Y.M., V.B.P., and J.S.S. performed research; A.F.G. and J.W. contributed new reagents/analytic tools; C.J., A.F.G., V.S., N.K.J., D.P., and W.Y. analyzed data; and C.J., A.F.G., V.S., N.K.J., D.P., B.L., J.W., Y.M., V.B.P., J.S.S., R.A., W.Y., and H.-k.M. wrote the paper.

Reviewers: R.M.W., Columbia University; and C.Y., Washington State University.

The authors declare no conflict of interest.

Freely available online through the PNAS open access option.

[1]To whom correspondence should be addressed. Email: hmao@ciw.edu.

This article contains supporting information online at www.pnas.org/lookup/suppl/doi:10.1073/pnas.1700049114/-/DCSupplemental.

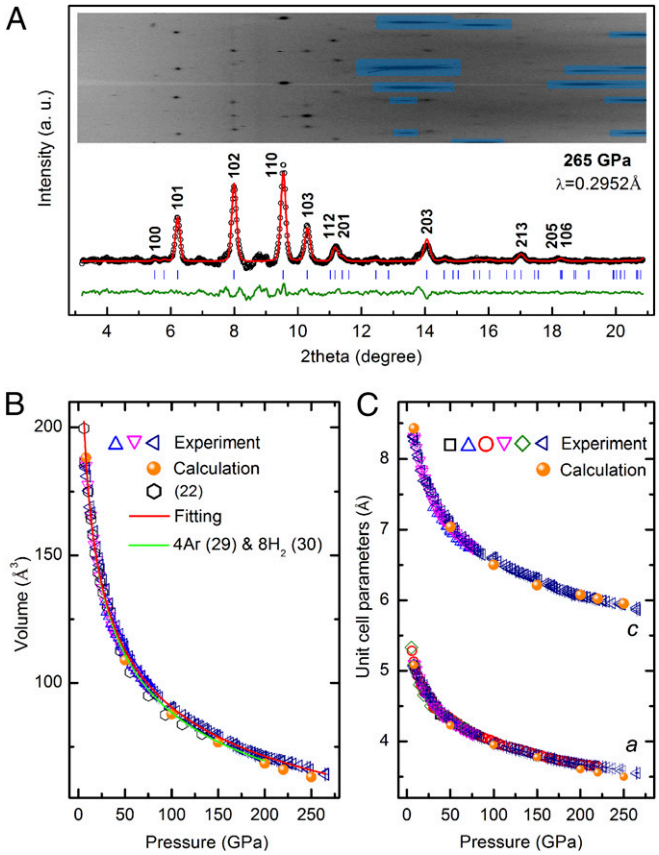

Fig. 1. (*A*) LeBail full-profile fitting of XRD pattern collected with rotating DAC by ±10° at 265 GPa. (*Inset*) Caked raw image. Masked regions (semi-transparent blue) are saturated diffraction peaks from diamond. (*B*) EOS of $Ar(H_2)_2$. (*C*) Cell parameters of $Ar(H_2)_2$ at pressures. Six samples were used to determine cell parameter *a*. Three of the six samples were used to determine both *a*, *c*, and unit cell volume. This is due to preferred orientations of $Ar(H_2)_2$ crystals formed under pressure (*SI Appendix*).

Synchrotron XRD measurements of $Ar(H_2)_2$ were performed up to 265 GPa to examine the evolution of the crystal structure with pressure. The XRD patterns can be indexed well with the $MgZn_2$-type model up to the highest pressure achieved (Fig. 1*A*). We did not observe the predicted phase with a $CeCu_2$-type structure, possessing a significantly lower lattice symmetry, at 55–70 GPa (23). Another predicted phase transition to the AlB_2-type structure (hexagonal lattice) at 250 GPa (22, 24) was also ruled out. The $MgCu_2$-type structure model, predicted as a low-temperature phase (27), was also examined and found inconsistent with our experimental data (see *SI Appendix* for details regarding the inapplicability of the AlB_2- and $MgCu_2$-type models).

The unit cell volume and cell parameters of $Ar(H_2)_2$ shift smoothly with increasing pressure, as shown in Fig. 1 *B* and *C*, indicating no change of stoichiometry. The pressure–volume data were fit using a third-order Vinet EOS (28) with constrained $V_0 = 480.868$ Å^3, which is the sum of V_0(Ar) (29) and $V_0(H_2)$ (30). We obtained $K_0 = 0.36(2)$ GPa, $K_0'=7.64$ (6), where V_0, K_0, and K_0' are the volume at ambient conditions, isothermal bulk modulus, and its first pressure derivative, respectively. These values are comparable to those of phase I of H_2, $K_0 = 0.162$ GPa and $K_0'= 6.813$ (30). It is interesting to note that the volume of $Ar(H_2)_2$ becomes slightly larger than the sum of the volumes of Ar (29) and H_2 (30) at pressures above 13.9 GPa (Fig. 1*B*). This is in contrast to $SiH_4(H_2)_2$, which shows a smaller volume compared with the sum of its components (19). The "shrunk" volume in $SiH_4(H_2)_2$ was suggested as the indication of a positive chemical pressure on H_2 molecules, associated with a significantly softened H_2 vibron mode compared with pure H_2. The question then arises whether the observation of an "expanded" unit cell of $Ar(H_2)_2$ infers an effect of negative chemical pressure on the H_2 molecules.

We performed Raman spectroscopy measurements to examine the behaviors of H_2 molecules in $Ar(H_2)_2$ under compression. At low pressures, $Ar(H_2)_2$ exhibits roton modes characteristic of free rotating H_2 molecules (*SI Appendix*, Fig. S5*A*), in agreement with the previous report (26). A previously unreported phonon mode with a weak intensity was resolved in our data. At high frequencies, two weak sidebands were observed besides the strong vibron (ν_1), with one at lower frequency (ν_2) and the other at higher frequency (ν_3), shown in Fig. 2*A*. The ν_1 mode was reported in all previous Raman studies (20, 26, 31) and the ν_3 mode was observed in ref. 31. The different vibrons are not attributed to different crystallographic sites due to the mismatch between the intensity ratio (intensities of sidebands are less than 1% of that of the main vibron ν_1) and the number ratio of molecules sitting on *2a* and *6h* sites in the unit cell (1:3). Thus, we assumed that due to the proximity of the intramolecular distances, the vibrons corresponding to molecules in *2a* and *6h* sites are indistinguishable in frequency at low pressures. The pressure-dependent frequency shift of the ν_3 mode is consistent with that of infrared vibron (Fig. 2*A*) (21, 26), suggesting that the ν_3 mode stems from folding of the Brillouin zone, which makes it Raman active (16, 32). The presence of the Raman-forbidden ν_2 mode is not clear and is tentatively assigned to the additional molecular ordering related to the diffraction rods observed in XRD.

Under further compression, the ν_1 mode shows a monotonic blue-shift up to at least 216 GPa. At 216 GPa the ν_1 mode splits, firstly indicated by a peak broadening of 37% compared with the previous pressure point (Fig. 2*B*). The splitting ($\Delta\nu$) increases from 14 cm^{-1} at 216 GPa to 57 cm^{-1} at 358 GPa (Fig. 2*C*). At 216 GPa

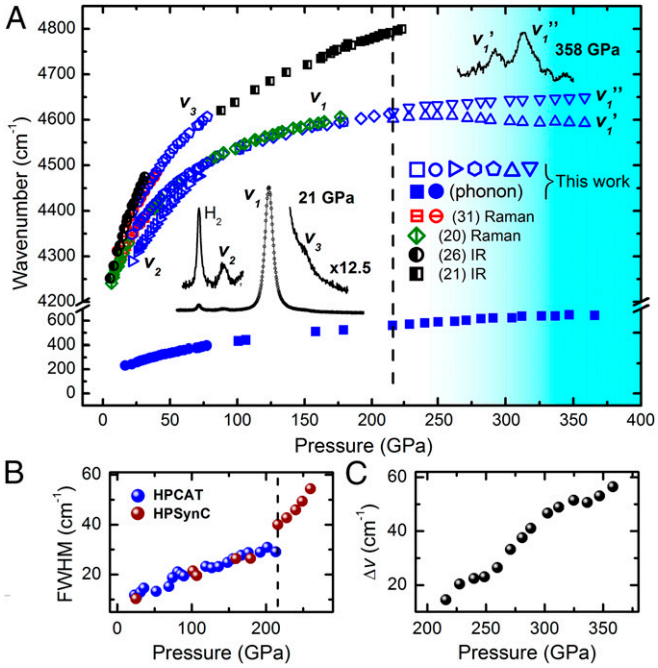

Fig. 2. (*A*) Frequency shift of Raman modes of $Ar(H_2)_2$ with compression. Dashed line indicates vibron split. Two inset spectra show vibron modes at 21 GPa (with magnification) and 358 GPa, respectively. (*B*) Peak width of the vibron mode at pressures by treating the broadened band as a single peak. Dashed line indicates the abrupt broadening. Symbols in different colors represent data collected using different Raman systems. (*C*) Separation between split vibrons at pressures.

where the vibron splits, the shift of phonon is smooth and remains positive throughout the measured pressure range (Fig. 2*A*). This is consistent with the continuity of structural parameters from XRD results at the conditions of vibron splitting and further supports that a possible phase transition at 216 GPa is not reconstructive. At 358 GPa, both vibrons are still present, as shown in Fig. 2*A*, indicating that no molecular dissociation occurs.

Here we discuss the origin of the vibron split in $Ar(H_2)_2$. The observed splitting indicates that there is a sizable difference in intramolecular distances between the H_2 molecules of two kinds that are present in the unit cell of $Ar(H_2)_2$. Generally, an abrupt vibron splitting can be caused by a lowering of the lattice symmetry, a change of composition, or a change of the molecular rotational state. Because a change of lattice symmetry or stoichiometry has been excluded as discussed previously, we propose that the vibron splitting is related to rotational ordering of the H_2 molecules. The *2a* and *6h* molecules which are rotationally disordered at low pressures experience different crystal fields under compression. Thus, it is natural to expect that this disparity results in the breaking of the rotational symmetry (the disordered orientation state). Similar observations of discontinuity in vibron frequencies can also be found in orientational transitions in H_2, D_2 (5, 32), and N_2 (33). In addition, our DFT calculations based on a model with all molecules aligned along the *c* axis (*c*-aligned) resolve different intramolecular bond lengths between *2a* and *6h* H_2 molecules, with the difference increasing with pressure (*SI Appendix*, Fig. S6*A*). This result qualitatively agrees with our observation in the Raman data (the calculation also reproduces EOS consistent with the XRD data), suggesting that this might be a model for the orientational ordering above 216 GPa. Further IR measurements above 220 GPa are expected to provide more constraints on the orientational state of H_2 molecules in $Ar(H_2)_2$.

The effect of Ar on the intermolecular interactions of H_2 in $Ar(H_2)_2$ is analyzed from the structural point of view compared

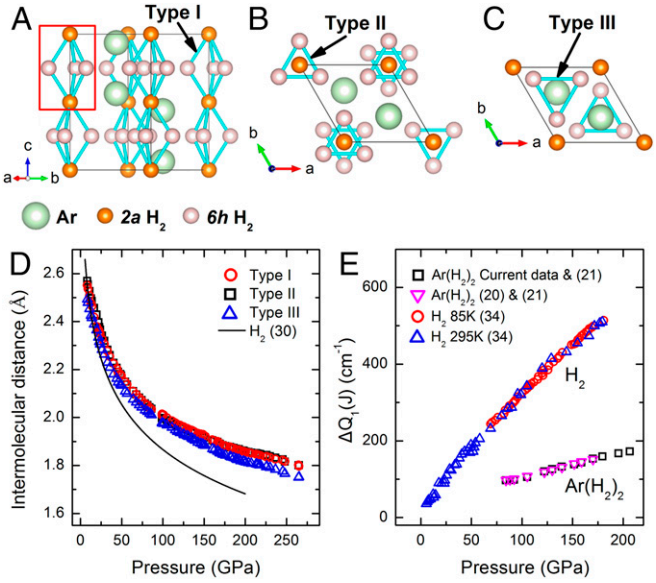

Fig. 3. (*A*–*C*) Schematic of nearest-neighbor intermolecular distances between H_2 molecules in $Ar(H_2)_2$. Cyan bars highlight intermolecular distances. There are three types of distances with close values. Intermolecular distance here refers to the distances between mass centers of H_2 molecules. Smaller spheres represent the molecular mass centers. Red box in *A* highlights a trigonal bipyramidal unit composed of five H_2 molecules. (*D*) Comparison of pressure-dependent intermolecular distance between $Ar(H_2)_2$ and phase I of H_2. The distances between H_2 molecules in $Ar(H_2)_2$ were calculated using the experimentally measured EOS and the theoretically determined positions of H_2 mass centers. (*E*) Comparison of $Q1(J)_{IR}$-$Q1(J)_{Raman}$ between $Ar(H_2)_2$ and phase I of H_2.

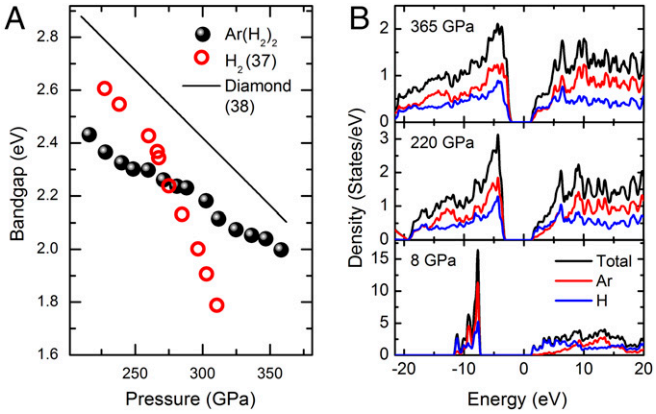

Fig. 4. (*A*) Evolution of the indirect bandgap of $Ar(H_2)_2$ with compression. (*B*) Calculated projected DOS of $Ar(H_2)_2$ at pressures.

with solid H_2. On the unit cell edges of $Ar(H_2)_2$, H_2 molecules can be considered as forming trigonal bipyramidals: three *6h* molecules form a triangle ring and two *2a* molecules reside respectively on the top and bottom of the ring (Fig. 3*A*). The trigonal bipyramidals are interconnected by their vertices along the axial direction, forming long chains along the *c* axis of the unit cell. This quasi-1D anisotropy of H_2 sublattice was considered to facilitate the insulator to metal transition (22). However, a direct comparison of the H_2 sublattice in $Ar(H_2)_2$ to the lattice of H_2 phase I shows that the coordination number of H_2 molecules (by nearest H_2 neighbors) in $Ar(H_2)_2$ is only 50% of that in H_2 phase I [6 for $Ar(H_2)_2$ and 12 for H_2 phase I]. Meanwhile, as shown in Fig. 3*D*, the closest intermolecular distances of H_2 molecules in $Ar(H_2)_2$ are larger than in phase I of H_2 (30) at the same pressure. Together the decreased coordination number and the increased intermolecular distance of H_2 molecules in $Ar(H_2)_2$ explain the effects of reduced phonon frequency and reduced vibron splitting between Raman and IR modes (see below). The intermolecular interaction between H_2 molecules inferred from the frequency difference between the IR vibron and the Raman vibron $Q1(J)_{IR}$-$Q1(J)_{Raman}$ (5, 34), denoted as $\Delta Q1(J)$, also suggests weaker intermolecular interactions in $Ar(H_2)_2$ compared with H_2 (Fig. 3*E*).

It is noteworthy that the triangular ring motif of molecules is a common and interesting feature of the recently proposed structure models of phases III and IV of H_2 (35, 36). For example, in the Cc structure model of phase IV (36), there is a graphene-like "atomic layer," within which three adjacent H_2 molecules form a ring, exhibiting strong intermolecular interactions (proton tunneling). This atomic layer feature was associated with a vibron mode which significantly softens and broadens with increasing pressure (37). Although the *6h* H_2 molecules in $Ar(H_2)_2$ also form H_2-only layers with triangle ring units (Fig. 3 *B* and *C*), no spectroscopic feature characterizing the atomic layer was observed in $Ar(H_2)_2$ (*SI Appendix*, Fig. S7). The absence of the atomic layer in $Ar(H_2)_2$ is attributed primarily to the increased intermolecular distance and possibly to a different pattern of molecular orientation as well.

To explore the electronic properties of $Ar(H_2)_2$ under high pressure, we measured the optical absorption of $Ar(H_2)_2$ and also calculated its projected density of states (PDOS). The bandgap of $Ar(H_2)_2$ becomes measurable above 216 GPa (*SI Appendix*, Fig. S8) and decreases with further compression to ~2.0 eV at 358 GPa, as shown in Fig. 4*A*. Measured values are lower than the bandgap of diamond (38) within the pressure range. Therefore, we consider our measurements representing the bandgap of $Ar(H_2)_2$. The observation of a visually transparent sample at 358 GPa (*SI Appendix*, Fig. S8) is also consistent with the measurements. A linear extrapolation of the bandgap to higher pressure suggests a bandgap closure at 1,020 ± 40 GPa, which is much higher than that

predicted for pure H_2 (near 400 GPa) (6), and in a qualitative agreement with the calculation (25) assuming metallization of $Ar(H_2)_2$ in the $MgZn_2$-type structure. The calculated PDOS, shown in Fig. 4*B*, shows increased dispersion of both the valence band and conduction band with compression, contributing to the decreased bandgap.

In addition, a charge analysis was performed based on an Ar4H36 cluster model to examine the interactions between Ar and H_2 at high pressure. The model is based on the relaxed coordinates from the VASP calculation (*c*-aligned). The results show an increased charge transfer from Ar to H_2 with pressure, reaching up to 0.17 e/atom on Ar at 365 GPa. It has been reported that the bond distance of HAr+, obtained by hollow-cathode discharges in a gas mixture of Ar with small amounts of H_2, is 1.28 Å (39). Comparing to this value, the closest Ar–H distance in our *c*-aligned model at 365 GPa is 1.75 Å. which is substantially larger. As a reference, the sum of covalent radii and van der Waals radii of Ar and H (ambient pressure) are 1.47 Å (40) and 3.03 Å (41), respectively, at ambient conditions. The results indicate that the valence orbitals of Ar and H are partially mixed at ultrahigh pressures, but no new bond has been created. Additionally, it has been predicted that in LiH_6 the charges transferred from Li can partially fill the σ_u^*-band of hydrogen thus facilitating metallization (13). Such an effect in $Ar(H_2)_2$ may not be as prominent because of the yet-limited charge transfer. *SI Appendix* includes more details and discussion about the charge analysis.

In summary, we have studied $Ar(H_2)_2$ by XRD up to 265 GPa and by Raman spectroscopy and optical absorption spectroscopy up to 358 GPa using DAC techniques. Metallization is not observed and H_2 preserves its molecular form until the highest pressure. A phase transition is revealed at 216 GPa, signified by the splitting of Raman vibron with no change in the lattice symmetry. It is likely accompanied by at least partial ordering of H_2 molecules, supported by theoretical calculations. Our study sheds conclusive light in the wake of several conflicting reports in the literature regarding the crystal structure and metallization of $Ar(H_2)_2$ at ultrahigh pressure. We show that the "Ar doping" introduces a negative chemical pressure for hydrogen molecules, depleting intermolecular interactions and causing the bandgap closure moving to high pressures.

Materials and Methods

A gas mixture of Ar and H_2 with a volume ratio of 1:3 and purity >99.9% was compressed to 0.17 GPa and loaded into DACs for measurements. All experiments were performed at room temperature. XRD experiments were conducted at beamline 13-IDD of GeoSoilEnviroCARS (GSECARS) and beamline 16-IDB of High Pressure Collaborative Access Team (HPCAT) at the Advanced Photon Source, Argonne National Laboratory. Pressures were measured using the gold standard (42). XRD data were recorded using Mar165 CCD detectors. The Raman and optical absorption measurements were conducted using confocal micro-Raman systems at High Pressure Synergetic Consortium at the Advanced Photon Source (HPSynC) (659.5 nm) and HPCAT (532.1 nm) with the backscattering geometry and CCD cameras. Pressures were measured using the diamond Raman edge (43). DFT-based calculations with Perdew–Burke–Ernzerhof exchange–correlation functional were performed under generalized gradient approximation (44, 45) as implemented in the Vienna Ab initio Simulation Package (VASP) (46). A plane-wave cutoff of 700 eV was used in our calculation. The calculations of PDOS and charge analysis were performed using the SIESTA (47) and Gaussian 09 programs (48), respectively.

ACKNOWLEDGMENTS. The authors give thanks to R. Ferry for help with gas-loading system of the diamond anvil cell samples, and G. Shen and Y. Ding for useful discussions. High Pressure Collaborative Access Team (HPCAT) operations are supported by the US Department of Energy (DOE)-NNSA under Award DE-NA0001974 and by the DOE-BES under Award DE-FG02-99ER45775, with partial instrumentation funding by the National Science Foundation (NSF). A.F.G. and V.B.P. are grateful for NSF Award MRI EAR/IF1531583. GeoSoilEnviroCARS is supported by the NSF—Earth Sciences (Grant EAR-1128799) and Department of Energy—Geosciences (Grant DE-FG02-94ER14466). A.F.G. was partially supported by Chinese Academy of Sciences Visiting Professorship for Senior International Scientists Grant 2011T2J20 and Recruitment Program of Foreign Experts. Use of the Advanced Photon Source was supported by the US Department of Energy, Office of Science, Office of Basic Energy Sciences under Contract DE-AC02-06CH11357. Computational resources were provided from Swedish National Infrastructure for Computing (Project SNIC-2015-10-19). V.S. acknowledges funding from the European Erasmus Fellowship program. R.A. acknowledges support from the Swedish Research Council.

1. Grochala W, Hoffmann R, Feng J, Ashcroft NW (2007) The chemical imagination at work in very tight places. *Angew Chem Int Ed Engl* 46(20):3620–3642.
2. Ashcroft NW (1968) Metallic hydrogen: A high-temperature superconductor? *Phys Rev Lett* 21(26):1748–1749.
3. Babaev E, Sudbø A, Ashcroft NW (2004) A superconductor to superfluid phase transition in liquid metallic hydrogen. *Nature* 431(7009):666–668.
4. Silvera I (1980) The solid molecular hydrogens in the condensed phase: Fundamentals and static properties. *Rev Mod Phys* 52(2):393–452.
5. Mao H, Hemley R (1994) Transitions in solid hydrogen. *Rev Mod Phys* 66(2):671–692.
6. McMahon JM, Morales MA, Pierleoni C, Ceperley DM (2012) The properties of hydrogen and helium under extreme conditions. *Rev Mod Phys* 84(4):1607–1653.
7. Wigner E, Huntington HB (1935) On the possibility of a metallic modification of hydrogen. *J Chem Phys* 3:764–770.
8. Barbee TW, 3rd, Garcia A, Cohen ML, Martins JL (1989) Theory of high-pressure phases of hydrogen. *Phys Rev Lett* 62(10):1150–1153.
9. Dalladay-Simpson P, Howie RT, Gregoryanz E (2016) Evidence for a new phase of dense hydrogen above 325 gigapascals. *Nature* 529(7584):63–67.
10. Eremets MI, Troyan IA, Drozdov AP (2016) Low temperature phase diagram of hydrogen at pressures up to 380 GPa. A possible metallic phase at 360 GPa and 200 K. arXiv:1601.04479.
11. Ashcroft NW (2004) Hydrogen dominant metallic alloys: High temperature superconductors? *Phys Rev Lett* 92(18):187002–1.
12. Carlsson A, Ashcroft N (1983) Approaches for reducing the insulator-metal transition pressure in hydrogen. *Phys Rev Lett* 50(17):1305–1308.
13. Zurek E, Hoffmann R, Ashcroft NW, Oganov AR, Lyakhov AO (2009) A little bit of lithium does a lot for hydrogen. *Proc Natl Acad Sci USA* 106(42):17640–17643.
14. Kleppe AK, Amboage M, Jephcoat AP (2014) New high-pressure van der Waals compound $Kr(H_2)_4$ discovered in the krypton-hydrogen binary system. *Sci Rep* 4:4989.
15. Somayazulu MS, Finger LW, Hemley RJ, Mao HK (1996) High-pressure compounds in methane-hydrogen mixtures. *Science* 271:1400–1402.
16. Somayazulu M, et al. (2010) Pressure-induced bonding and compound formation in xenon-hydrogen solids. *Nat Chem* 2(1):50–53.
17. Strobel TA, Somayazulu M, Sinogeikin SV, Dera P, Hemley RJ (2016) Hydrogen-stuffed, quartz-like water ice. *J Am Chem Soc* 138(42):13786–13789.
18. Strobel TA, Chen XJ, Somayazulu M, Hemley RJ (2010) Vibrational dynamics, intermolecular interactions, and compound formation in GeH_4-H_2 under pressure. *J Chem Phys* 133(16):164512.
19. Strobel TA, Somayazulu M, Hemley RJ (2009) Novel pressure-induced interactions in silane-hydrogen. *Phys Rev Lett* 103(6):065701.
20. Loubeyre P, Letoullec R, Pinceaux J-P (1994) Compression of $Ar(H_2)_2$ up to 175 GPa: A new path for the dissociation of molecular hydrogen? *Phys Rev Lett* 72(9):1360–1363.
21. Hemley RJ (2000) Effects of high pressure on molecules. *Annu Rev Phys Chem* 51:763–800.
22. Bernard S, Loubeyre P, Zérah G (1997) Phase transition in $Ar(H_2)_2$: A prediction of metallic hydrogen organized in lamellar structures. *Europhys Lett* 37(7):477–482.
23. Yao Y, Klug D (2011) High-pressure phase transition and metallization in $Ar(H_2)_2$. *Phys Rev B* 83:020105.
24. Matsumoto N, Nagara H (2007) Ab initio calculations for high-pressure phases of $Ar(H_2)_2$. *J Phys Condens Matter* 19(36):365237.
25. Chacham H, Koiller B (1995) Band-gap closure of $Ar(H_2)_2$ under pressure. *Phys Rev B Condens Matter* 52(9):6147–6149.
26. Ulivi L, Bini R, Loubeyre P, LeToullec R, Jodl HJ (1999) Spectroscopic studies of the Ar $(H_2)_2$ compound crystal at high pressure and low temperatures. *Phys Rev B* 60(9):6502–6512.
27. Cazorla C, Errandonea D (2010) Ab initio study of compressed $Ar(H_2)_2$: Structural stability and anomalous melting. *Phys Rev B* 81:104108.
28. Vinet P, Ferrante J, Smith JR, Rose JH (1986) A universal equation of state for solids. *J Phys C Solid State Phys* 19:467.
29. Errandonea D, Boehler R, Japel S, Mezouar M, Benedetti LR (2006) Structural transformation of compressed solid Ar: An x-ray diffraction study to 114 GPa. *Phys Rev B* 73:92106.
30. Loubeyre P, et al. (1996) X-ray diffraction and equation of state of hydrogen at megabar pressures. *Nature* 383:702–704.
31. Hemley RJ, Somayazulu MS, Goncharov AF, Mao HK (1998) High-pressure Raman spectroscopy of Ar-H_2 and CH_4-H_2 van der Waals compounds. *Asian J Phys* 7(2):319–322.
32. Goncharov AF, Eggert JH, Mazin II, Hemley RJ, Mao Hk (1996) Raman excitations and orientational ordering in deuterium at high pressure. *Phys Rev B Condens Matter* 54(22):R15590–R15593.
33. LeSar R, et al. (1979) Raman spectroscopy of solid nitrogen up to 374 kbar. *Solid State Commun* 32(2):131–134.
34. Hanfland M, Hemley RJ, Mao Hk (1993) Novel infrared vibron absorption in solid hydrogen at megabar pressures. *Phys Rev Lett* 70(24):3760–3763.
35. Pickard C, Needs R (2007) Structure of phase III of solid hydrogen. *Nat Phys* 3:473.
36. Liu H, Ma Y (2013) Proton or deuteron transfer in phase IV of solid hydrogen and deuterium. *Phys Rev Lett* 110(2):025903.

37. Howie RT, Guillaume CL, Scheler T, Goncharov AF, Gregoryanz E (2012) Mixed molecular and atomic phase of dense hydrogen. *Phys Rev Lett* 108(12):125501.
38. Ruoff AL, Luo H, Vohra YK (1991) The closing diamond anvil optical window in multimegabar research. *J Appl Phys* 69(9):6413–6416.
39. Johns JWC (1984) Spectra of the protonated rare gases. *J Mol Spectrosc* 106:124–133.
40. Cordero B, et al. (2008) Covalent radii revisited. *Dalton Trans* (21):2832–2838.
41. Alvarez S (2013) A cartography of the van der Waals territories. *Dalton Trans* 42(24): 8617–8636.
42. Anderson OL, Isaak DG, Yamamoto S (1989) Anharmonicity and the equation of state for gold. *J Appl Phys* 65(4):1534.
43. Akahama Y, Kawamura H (2010) Pressure calibration of diamond anvil Raman gauge to 410 GPa. *J Phys Conf Ser* 215:12195.
44. Hohenberg P, Kohn W (1964) Inhomogeneous electron gas. *Phys Rev* 136:864.
45. Perdew JP, Burke K, Ernzerhof M (1996) Generalized gradient approximation made simple. *Phys Rev Lett* 77(18):3865–3868.
46. Kresse G, Furthmüller J (1996) Efficient iterative schemes for ab initio total-energy calculations using a plane-wave basis set. *Phys Rev B Condens Matter* 54(16):11169–11186.
47. Soler JM, et al. (2002) The SIESTA method for ab initio order-N materials simulation. *J Phys Condens Matter* 14:2745–2779.
48. Frisch MJ, et al. (2009) *Gaussian 09, Revision E.01* (Gaussian, Inc., Wallingford, CT).